A Simple Theoretical Model Explains Dynein's Response to Load

Yi Qin Gao
Department of Chemistry, Texas A&M University, College Station, Texas 77843

ABSTRACT Recent experiment showed that cytoplasmic dynein 1, a molecular motor responsible for cargo transport in cells, functions as a gear in response to external load. In the presence of vanishing or small external load, dynein walks with 24- or 32-nm steps, whereas at high external load, its step size is reduced to 8 nm. A simple model is proposed to account for this property of dynein. The model assumes that the chemical energy of ATP hydrolysis is used through a loose coupling between the chemical reaction and the translocation of dynein along microtubule. This loose chemomechanical coupling is represented by the loosely coupled motions of dynein along two different reaction coordinates. The first reaction coordinate is tightly coupled to the chemical reaction and describes the protein conformational changes that control the chemical processes, including ATP binding and hydrolysis, and ADP-Pi release. The second coordinate describes the translocation of dynein along microtubule, which is directly subject to the influence of the external load. The model is used to explain the experimental data on the external force dependence of the dynein step size as well as the ATP concentration dependence of the stall force. A number of predictions, such as the external force dependence of speed of translocation, ATP hydrolysis rate, and dynein step sizes, are made based on this theoretical model. This model provides a simple understanding on how a variable chemomechanical coupling ratio can be achieved and used to optimize the biological function of dynein.

INTRODUCTION

Dynein is among one of the three families of molecular motors that are responsible for the motility of eukaryotic cells (1–5). The other two, kinesin and myosin, are much better characterized and their functions better understood. Although dynein has been known as the force-generating element in cells since 1965 and there have been significant advances in the structural and mechanistic studies of this motor protein (6–9), due to the lack of atomic detailed structural information, our understanding of the mechanism of cargo transport by dynein is still very limited. This relative slow advance in the studies of dynein is partly due to its large and complex structure. To maintain a complete molecular activity, the required size of dynein is ~380 kDa (4), almost 10 times larger than that of kinesin. Its total molecular weight is ~1.2 MDa (4–9). Most structural information of dynein comes from electron microscopic (EM) studies. Dynein has a motor domain consisting of seven different globular subdomains, which together form a ring-like architecture surrounding a central cavity (8,9). Moreover, the dynein motor domain contains multiple nucleotide binding sites, unlike that of myosin or kinesin, which contains a single nucleotide binding site. Six out of the seven globular domains are AAA-like (ATPase associated with diverse cellular activities) domains, and are named AAA1-AAA6. Four of the six AAA domains, AAA1-AAA4, bind ATP with different binding affinities (9–11). AAA1 appears to contain the active site for ATP hydrolysis, although AAA2-AAA4 also have some catalytic activity (3,4,6,11), and experiments indicated that AAA3 is essential for the dynein-induced microtubule gliding activity (4,12).

The other structural elements that are important in force generation by dynein include the microtubule binding stalk (MT stalk), an unusual 13-nm-long structure projected out of the ring-like motor domain, and the stem, another elongated projection (1,4,8,9). The MT stalk contains a small bulky structure that is responsible for dynein binding to the microtubule and the stem regulates the binding of dynein with different cargoes. Both MT stalk and the stem are potential lever arms (1,8,9). In the EM image of dynein, the MT stalk and the stem point to different directions (8,9). Their orientations with respect to the motor domain were shown to depend on the dynein power-stroke state. In both axonemal and cytoplasmic dynein, after ATP hydrolysis and product release there is a rotation of the ring of the motor domain around the motor-stem junction (1,4,5,8). (In this article, we focus on the cytoplasm dynein 1 and use the term dynein for this species, unless otherwise stated). The motion of the motor domain with respect to the stem presumably forms one of the essential elements of the power stroke of dynein and is estimated to produce a movement of the motor domain along the microtubule of 15 nm (1,2). The step length is expected to be longer when the movement of the other lever arm formed by the MT stalk is taken into account (1). This overall appearance of the dynein structure is very different from that of myosin and kinesin, which have only one arm emerged from the catalytic domain (the motor domain contains both the nucleotide binding and the track binding sites).

Superficially, all protein motors using ATP as the energy source follow a similar strategy (4,5) in which the motor core binds and hydrolyzes ATP and coordinates these chemical processes with the conformational changes of the protein motor. The latter generates the mechanical movement of the motor. The chemical transitions in the motor domain regulate

Submitted August 23, 2005, and accepted for publication October 17, 2005.
Address reprint requests to Yi Qin Gao, E-mail: yiqin@mail.chem.tamu.edu.

0006-3495/06/02/811/11 $2.00
doi: 10.1529/biophysj.105.073189

the binding of motor with its track, such as the microtubule or the actin filament. Although there are still many uncertainties on how exactly the chemical energy is converted into mechanical energy, typically with a high efficiency, even for the better characterized systems such as myosin and kinesin, a large body of experimental data have been accumulated on the kinetics and mechanics of these protein motors. For example, experiments showed that both traditional kinesin (13) and myosin (at least myosin V) (14) walk by a hand-over-hand mechanism and there exists a tight coupling between the chemical and mechanical processes. Every ATP hydrolyzed generates an 8-nm movement of kinesin along the microtubule in a large range of external load (15–17). Cooperation between the two heads of kinesin is thought to be essential for its movement (15,17). Similarly, dynein also processes by 8-nm steps when it walks against a heavy load (18,19) and it was shown that a single-headed dynein is only able to bind and hydrolyze ATP but not able to move along the microtubule (20). However, recent single-molecule experiments (21) of dynein showed at least three aspects of the chemomechanical properties of dynein that are very different from kinesin.

The main difference between kinesin and dynein comes from their different responses to the externally applied force and to the variation of ATP concentration. Firstly, the stall force (the force applied in the direction opposite to the protein motion that prevents it from moving forward) is much less sensitive to the variation of ATP concentration for kinesin (16,17) than for dynein (21). When ATP concentration changes from 5 μM to 1 mM, the stall force increases by $\sim$20% for kinesin (17), whereas in the case of dynein it increases more than four times when ATP concentration changes from 0.1 to 1 mM (21). Secondly, the maximal stall force in the presence of saturating concentrations of ATP is significantly larger for kinesin ($>$8 pN) (16,17) than for dynein ($\sim$1.1 pN) (21). Thirdly and most interestingly, whereas kinesin exhibits a constant chemomechanical coupling ratio at all forces smaller than the stall force (the hydrolysis of each ATP molecule leads to a translocation of 8 nm, as discussed earlier), dynein's step size varies with the external load, namely, dynein switches gear in response to the external load (21,22). When the external force is large, the step size of dynein is 8 nm (18,19), the same as that of kinesin and is approximately the distance between the adjacent binding sites on microtubule (it was shown that kinesin and dynein bind at the same positions on a microtubule (23)). The step size of dynein increases with decreasing external force. When the external force vanishes, the step size of dynein is most likely to be 24 or 32 nm (21).

In the following, we present a simple theoretical model for the chemomechanical coupling involved in the walking of dynein. The theoretical framework used in this study is based on a ''thermal ratchet'' approach, similar to that used by Oster and co-workers in their studies of F-ATPase (24,25) and by Astumian and co-workers for kinesin (26), just to name a few of the most notable. Simple model potential energy surfaces taking into account the periodicity of the binding between the dynein and microtubule are used in this model. The distinctive feature of this model is that two different reaction coordinates (instead of one) are introduced so that the loose coupling between the chemical reaction (ATP hydrolysis) and the translocation of dynein along its microtubule track is taken into account. The first reaction coordinate describes the conformational changes that directly control the chemical reactions, including ATP binding and hydrolysis and ADP and Pi release, and thus can be considered tightly coupled to the usage of energy. Therefore, the motion along this reaction coordinate takes into account the conformational changes of dynein that influence the free-energy barriers for the chemical reactions that occur in the active ATP binding site. The motion along the second reaction coordinate, taken to be the position of dynein along microtubule, is also driven by energy (power stroke) generated from ATP hydrolysis. However, the chemical processes are not tightly coupled to the latter motion, i.e., the free-energy barriers of the chemical reactions are not directly controlled by the motion of dynein along microtubule. As a result, the external force influences directly the second but not the first type of motion (conformational changes). After this separation of motions, a loose instead of tight coupling exists between the translocation of dynein and its catalysis of ATP hydrolysis and the dynein step sizes vary with the external load. This model explains the experimentally observed ATP concentration dependence of the stall force and the external force dependence of the step sizes of dynein. It is also used to study the ATP concentration and external force dependence of the ATP hydrolysis rate and the walking velocity of dynein.

THEORETICAL MODEL

Description of the model

Because a tight coupling between the catalyzed ATP hydrolysis reaction and the physical translocation of a protein motor leads to a constant chemomechanical coupling ratio (e.g., the tight coupling of kinesin results in an 8-nm step for every ATP hydrolyzed (15)), to account for the variations in the chemomechanical coupling ratio of dynein, it is necessary to introduce a loose coupling between the chemical reaction and its physical movement. As discussed above, in this model the movement of dynein is described by two reaction coordinates, one of which describes the conformation of the dynein that controls the ATP hydrolysis reaction (e.g., the local conformation of the catalytic site); and the other describes the translocation of a dynein molecule along the microtubule. The conformation change of the catalytic core for the chemical reaction and the translocation along the microtubule are thus treated separately, with ATP hydrolysis being the common energy source. Hereinafter, the first coordinate is called the chemical reaction coordinate (α) and the second the physical reaction coordinate (x). The relation of chemical coordinate and the chemical transitions is the same as that between the reaction coordinate and chemical transitions in a tight coupling model (24,26). The essential features of the theoretical model include:

1. One ATP molecule is hydrolyzed per cycle of reaction, through which dynein goes through a series of chemical states defined by the

occupation of its active ATP hydrolysis site (there could be more than one site involved but the net result is that one solution ATP is hydrolyzed to yield ADP-Pi). At this stage, one cannot exclude the possibility that more than one ATP molecule (e.g., ATP hydrolysis at AAA4; (10)) is hydrolyzed every physical step of dynein. However, inclusion of ATP hydrolysis at another site changes either only the magnitude of drive force or the regulatory mechanism of dynein function (10) but not the concern of this article, the essential chemomechanical coupling mechanism. The possible regulatory roles of AAA2-AAA4 domains are discussed in a separate article (Y. Q. Gao, unpublished data). For simplicity, only three chemical states are considered explicitly in this model: the ATP (ADP-Pi), ADP, and empty states. The sequence of events in ATP-driven motion of dynein is described as follows: The binding of ATP to a dynein motor domain detaches its stalk domain from microtubule (5,27). ATP binding and the subsequent hydrolysis reaction (which together is taken as a single chemical state) and product release provide the energy for the conformational change in the catalytic core (described by the reaction coordinate α), as well as drive the translocation of dynein along the coordinate x. (In this powerstroke model, the energy is restored in the restrained conformation of dynein with an empty AAA1 binding site, the binding of ATP to AAA1 releases this constraint and allows dynein to move forward along microtubule.) The conformational change along the chemical reaction coordinate (e.g., the change of conformation of the catalytic core of the AAA1 domain) is required for the chemical transitions and in turn the chemical transitions induce the conformational changes in α. Each of the chemical states prefers a different conformation of the nucleotide binding site including the P-loop region (10). The chemical transitions occur in the following order: ATP binding and hydrolysis $\rightarrow$ Pi release $\rightarrow$ ADP release, with a conformational change in the α-coordinate after each of the chemical transitions. During this process of chemical energy release, dynein walks in the minus end along microtubule. At the same time of the translocation of dynein along microtubule, conformational changes coupled to the chemical transitions such as ADP and Pi release occur in the motor domain (along the α-coordinate). After Pi and ADP are released and the AAA1 domain becomes empty, the conformation of dynein in the α-coordinate returns to its poststroke (ATP-free) state and dynein rebinds microtubule. As a consequence, through this cycle of dynein conformational change along the α-coordinate, one ATP molecule has been hydrolyzed into ADP and Pi and dynein has displaced from its original position on microtubule.

2. ATP hydrolysis is assumed to be activated by dynein binding to microtubule. This assumption is in accordance with the experimental observation that the presence of microtubule stimulates the ATPase activity of dynein (10). The rates of other chemical transitions (binding of ATP and release of ADP-Pi) depend explicitly on α but not on x, so that the chemical reaction is not tightly coupled to the translocation of dynein (see Appendix for more details). The transitions between chemical states are random processes and the probabilities for the occurrence of these transitions are determined by the rate constants of the transitions.
3. The binding sites of dynein on microtubule are distributed according to the microtubule lattice structure with a separation distance of 8.1 nm. The chemical transitions of dynein (e.g, binding of ATP) induce the conformational changes along the α-coordinate, and the latter changes the binding affinity between the dynein and the microtubule. When dynein is at a poststroke state (e.g., the empty state), it binds preferably to one of the binding sites on microtubule. The binding of ATP and subsequent ATP hydrolysis at the active site of dynein bound to microtubule, which transforms dynein into a prestroke state, induces the conformational change of the motor domain (the α-coordinate). This change of dynein conformation reduces its binding affinity with microtubule and a power stroke is generated for dynein to displace in the minus direction of microtubule (the comparison of structures obtained in the presence of ADP + Vanadate and in the absence of nucleotide suggests that a power stroke may be produced when ADP and Pi are released in the ATP hydrolysis cycle (2,5,8)). This driving force is represented by a harmonic term in this study

$$V_{\mathrm{x,ATP}}(x) = \frac{K_{\mathrm{PS}}}{2}(x - x_{\mathrm{d}} - d_{\max})^2. \quad (1)$$

In Eq. 1, x_{d} is the position of dynein along x where ATP binding occurs, and $d_{\max}$ is the maximum displacement driven by the power stroke and has been estimated to be ~30 nm (21,28). The force constant K_{ps} is estimated using the experimental maximum stall force to be 0.04 pN nm^{-1} (see Appendix for detailed discussions). Dynein walks along a single protofilament.

4. Motions along both the chemical and physical reaction coordinates are continuous and are described by Langevin equations. The diffusion constants are assumed to be independent of the chemical states and are taken from experimental measurements. The potential of mean force that acts on the dynein molecule takes into account condition (3), and depends on the chemical state of dynein. Simplified model potentials are used in this study and they are given in the Appendix.

Equations of motions

The motion of dynein is described by its random movement along the reaction coordinates on the potential energy surface determined by its chemical state. After neglecting the inertia and balancing the forces on the motor including thermal fluctuations, the displacement of the motor in a time interval Δt can be written as (30)

$$x(t + \Delta t) - x(t) = (F_{\mathrm{x,i}}/\zeta_{\mathrm{x,i}})\Delta t + \Delta x(t), \quad (2)$$

and

$$\alpha(t + \Delta t) - \alpha(t) = (F_{\alpha,\mathrm{i}}/\zeta_{\alpha,\mathrm{i}})\Delta t + \Delta\alpha(t). \quad (3)$$

In Eqs. 2 and 3, $\zeta_{\mathrm{x,i}}$ and $\zeta_{\alpha,\mathrm{i}}$ are the friction constants for the motion along x- and α-directions, respectively. The terms $\Delta x(t)$ and $\Delta\alpha(t)$ are the random displacement due to the stochastic force and in the presence of white noise, they can be written as $\Delta x(t) = \sqrt{2D_{\mathrm{x,i}}\Delta t}R_1$ and $\Delta\alpha(t) = \sqrt{2D_{\alpha,\mathrm{i}}\Delta t}R_2$, respectively. $D = \zeta/k_{\mathrm{B}}\mathrm{T}$, k_{B} being the Boltzmann constant and T being the temperature, is the diffusion coefficient and Rs are random numbers. R_1 and R_2 are independent and each has a Gaussian distribution with a zero mean and a unitary standard deviation. In Eqs. 2 and 3, $F_{\mathrm{x,i}}$ and $F_{\alpha,\mathrm{i}}$ are the forces acting along the coordinates x and α, respectively. These forces can be further written as

$$F_{\mathrm{x,i}} = -\partial V(x, \alpha; i)/\partial x - F_{\mathrm{x,ext}};$$
$$F_{\alpha,\mathrm{i}} = -\partial V(x, \alpha; i)/\partial\alpha - F_{\alpha,\mathrm{ext}},$$

where $V(x, \alpha; i)$ is the two-dimensional potential of mean force acting on the motor when it is at chemical state i and F_{ext} is the external load (e.g., the force applied through an optical trap). The F_{ext} is defined so that it is positive when the force is in the opposite direction of dynein motion. The detailed expressions of $V(x,\alpha;i)$ are given in the Appendix. Because stochastic forces have been taken into account through the terms $\Delta x(t)$ and $\Delta\alpha(t)$, F_{ext} does not include frictional forces. The detailed potential energy functions, diffusion constants, and the rate constants of chemical transitions are given in the Appendix.

RESULTS AND COMPARISON WITH EXPERIMENTS

Motion of dynein in the absence of external force

A typical trajectory is given in Fig. 1 *a* for a dynein moving along the microtubule track in the absence of external load. The average translocation speed of dynein obtained from the calculations is 0.51 μm/s and is consistent with the

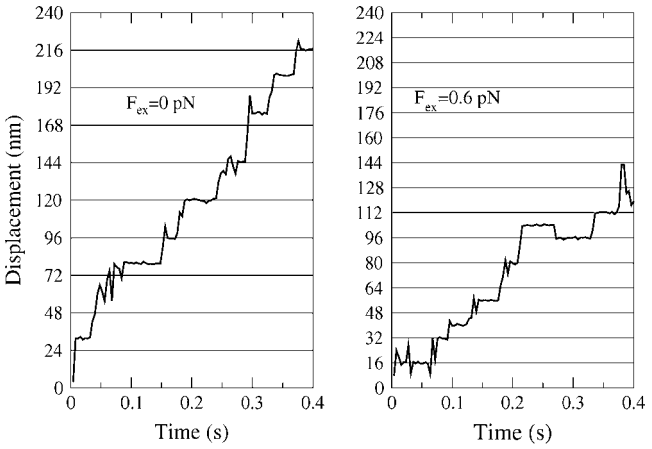

FIGURE 1 Calculated traces for the translocation of dynein along microtubule in the presence of constant external load. [ATP] = 1 mM, and $F_{ex} = 0$ pN (*left*), $F_{ex} = 0.6$ pN (*right*). The time step used in the calculation is 0.01 μs.

experimental value of ~0.5 μm/s (29). The speed of the dynein motion in the absence of external load as a function of ATP concentration is fitted to a simple Michaelis-Menten kinetics (Fig. 2) with a maximum speed, V_{cat}, of 0.51 μm/s and a K_M of 38 μM. This value of K_M is in reasonable agreement with the experimental results obtained for both cytoplasm dynein (10,31) and the monomeric dynein a (32). It is also seen from the trajectory that in the absence of external force dynein takes large step sizes (16, 24, or 32 nm), consistent with experimental observations.

Decrease of step lengths and walking speed with increasing forces

To study the influence of the external load on the walking patterns and speed of dynein, two types of calculations were performed. In the first simulation, an additional force term of $-kx$ is added to $F_{x,i}$ in Eq. 2, where k is a force constant. This simulation is used to mimic the experimental forces applied through an optical trap. We carried out simulations on the translocation of dynein on the microtubule against this applied force at different solution concentrations of ATP. Some typical trajectories are shown in Fig. 3. It is seen that, consistent with the experimental observations, dynein takes large step sizes (24 or 32 nm) when the displacement is small (which corresponds to a small external load). When dynein displaces further away from the origin, the force increases and dynein step size decreases. In the presence of sufficiently large external forces the forward motion of dynein ceases and occasionally moves backward. It is also seen from Fig. 3 that the stall force of dynein in the presence of 1 mM ATP is ~1 pN (displacement of ~80 nm) and on average the forward movement of dynein ceases at smaller forces at lower ATP concentrations, all in agreement with experimental observations (21).

For the characterization of the external force dependence of the dynein motion, simulations were carried out in which constant external forces were applied. Fig. 4 shows that the speed of dynein decreases with increasing external load, for all ATP concentrations used in the calculations. The force dependence of dynein speed is shown in Fig. 5 for various concentrations of ATP. The stall forces are estimated as the force at which the speed of dynein becomes zero using linear fits of the calculated data. Although there do not exist experimental data on the force dependence of walking speed for cytoplasm dynein 1 and our results are subject to tests of experiments, experiments on inner-arm axonemal dynein did show that its translocation speed decreases approximately linearly with the external force in the presence of both 5 and 100 μM of ATP (33). Our calculated results are generally consistent with this experimental observation (see Fig. 5). The calculated stall forces are shown in Fig. 6 for different concentrations of ATP, in comparison with experimental results. A clear dependence of the stall force on the ATP concentration is seen from that figure: the stall force is ~1.1 pN at high concentrations of ATP

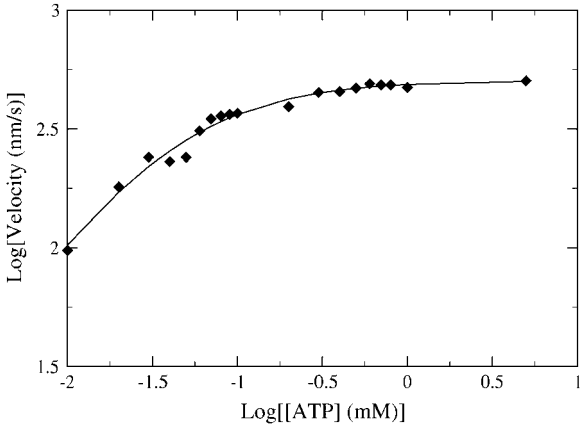

FIGURE 2 A log-log plot for the speed of dynein as a function of ATP concentration in the absence of external load. The calculated results were fitted to a Michaelis-Menten kinetics with $V_{cat} = 0.51$ μm/s and $K_M = 38$ μM.

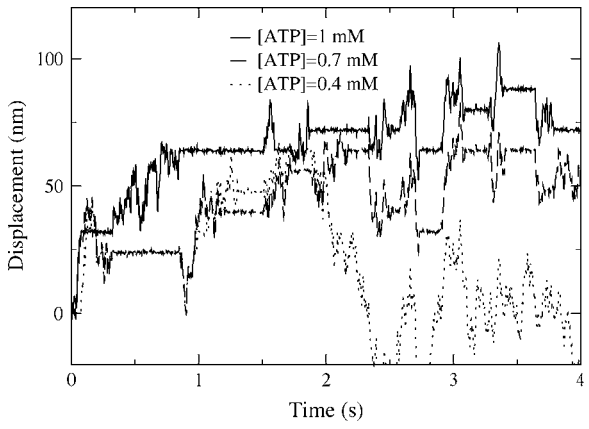

FIGURE 3 Calculated traces of dynein motion in the presence of an external force with a form of kx, which mimics the force exerted from an optical trap; $k = 0.011$ pN nm^{-1}. ATP concentrations are 1, 0.7, and 0.4 mM, respectively.

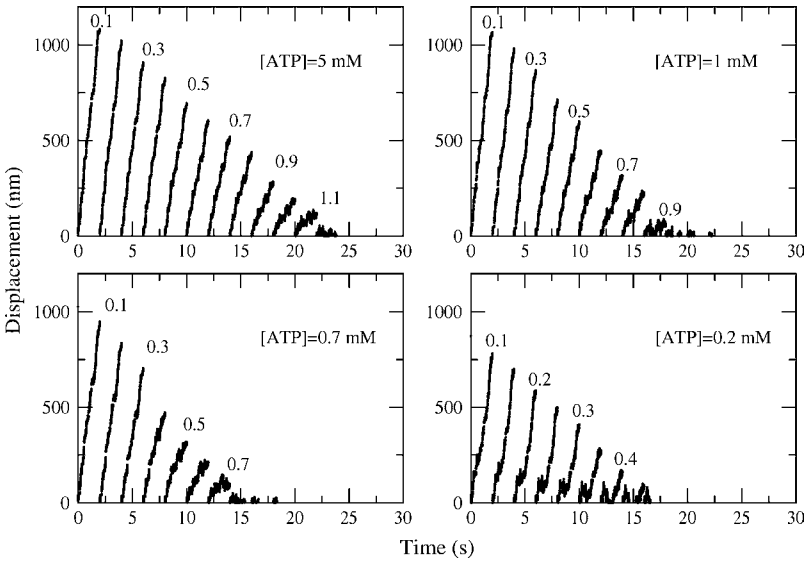

FIGURE 4 Calculated traces of dynein motion in the presence of various ATP concentrations and various constant external loads. Each of the traces represents a 2-s trajectory. Therefore, the final positions on the trajectories indicate the velocity.

(5 mM) and becomes ~0.4 pN at low concentrations of ATP (~0.1 mM). The stall force decreases approximately linearly with ATP concentration in the range of 0.1–1 mM, consistent with the experimental results, although the experiments were carried out with forces that vary with dynein displacement (21) instead of constant forces.

To quantitatively characterize the force dependence of step size on the external force, trajectories obtained in the presence of different external forces are analyzed. As seen from Fig. 1 the increase of the external force from 0 to 0.6 pN not only decreases the speed of motion, but also decreases the sizes of the steps. This dependence of step size on external force is more clearly seen in the pair distribution functions given in Fig. 7. In Fig. 7, when the external load vanishes, the highest peaks occur at 24, 48 = 2 × 24 nm, indicating that the most abundant steps at low external loads are of the size of 24 nm. When the external increases, the distribution shifts toward smaller values of displacements. When the external force is 0.6 pN, the highest peaks occur at 16 and 32 = 2 × 16 nm, whereas the count of 24-nm steps becomes significantly smaller, indicating that the 24-nm steps become less frequent and 16-nm steps are more abundant. When the external force is large (close to the maximum stall force of 1.1 pN) dynein takes 8-nm steps. These results are in good agreement with experiments, given that the diffusion constant of dynein was taken from independent experiments of Wang and Sheetz (29).

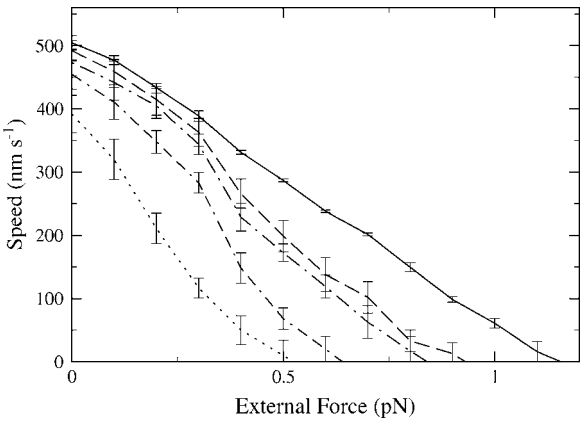

FIGURE 5 The speed of dynein motion averaged from five 2-s calculations as a function of external load for various ATP concentrations (from top to bottom, 5, 1, 0.6, 0.4, and 0.2 mM, respectively).

DISCUSSIONS

The dynein as a gear and its thermodynamic efficiency

A simple model is presented in this article to study how dynein functions as a gear in response to external force when

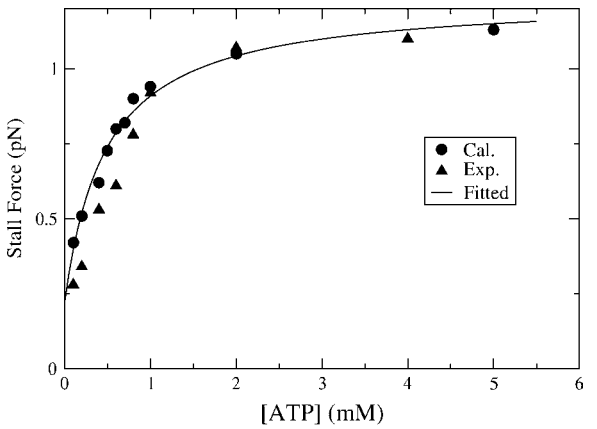

FIGURE 6 Stall forces obtained from linear fits of data on the external force dependence of dynein speed (such as those given in Fig. 4) as a function of ATP concentration. The experimental data are from Iyadurai et al. (20). The calculated data were fitted to a function $F_{stall} = 0.22 + 1.02[ATP]/(0.48 + [ATP])$, in units of piconewtons.

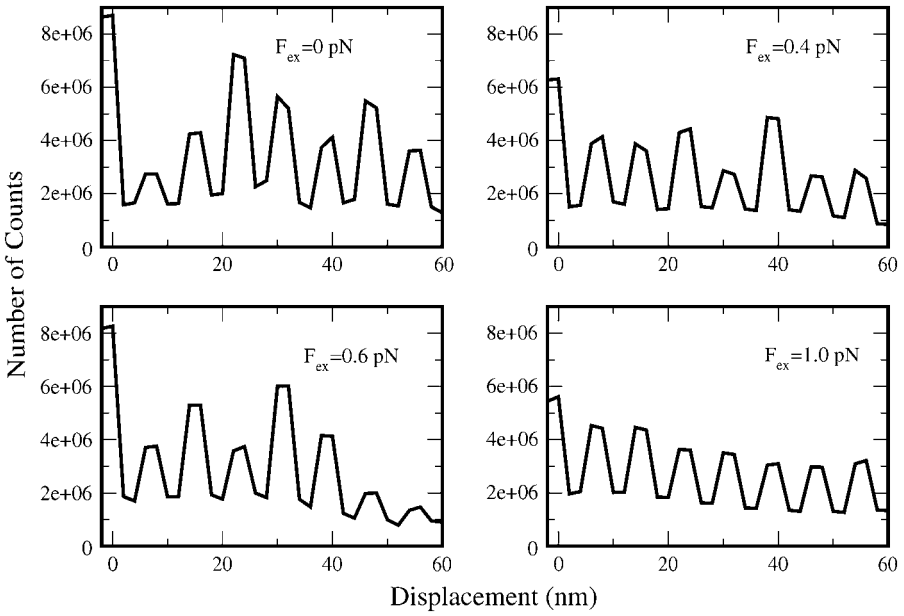

FIGURE 7 Pairwise distribution functions calculated in the presence of an external load of the magnitude of (*top left*) 0 pN, (*top right*) 0.4 pN, (*bottom left*) 0.6 pN, and (*bottom right*) 1.0 pN. The ATP concentration is 1 mM for the top two panels and the bottom left panel, and is 5 mM for the bottom right panel.

it transports cargoes along microtubule. One of the essential elements of this model is that the chemical reaction is not tightly but loosely coupled to the physical translocation of dynein. The loose coupling between the chemical reaction and the linear motion of dynein along the microtubule is modeled by invoking two reaction coordinates, x and α. The former is used to describe the displacement of dynein on the microtubule and the latter serves as the reaction coordinate for the conformational change that controls the rates of chemical transitions. The chemical energy restored in ATP is released through these chemical transitions that include ATP binding, ATP hydrolysis, and ADP-Pi release and drives the conformational changes of dynein in both x- and α-coordinates. The motions along the two reaction coordinates are largely independent except that the conformation of dynein motor domain, described by the α-coordinate, influences the binding affinity of dynein to microtubule. Because the force applied against the motion of dynein changes the potential energy surface along the x-coordinate and slows down the translocation of dynein along the microtubule but does not directly affect the conformational change along the reaction coordinate α, the relative speed of motion along the two coordinates vary with the external load. When the external force is small, dynein moves a long distance in the x-direction before its conformational change in the α-coordinate permits it to rebind microtubule. In the presence of a large external load, which decreases the driving force and slows down the motion in the x-direction, a cycle of conformational changes in the α-coordinate completes after a short displacement along x. Therefore, a smaller step size is observed.

The above argument can also be seen as follows. In the presence of a constant external force F_{ext}, which has a positive sign when it is applied opposing the motion of dynein, the potential energy profile (c.f. Eq. 1) along the x-coordinate reads

$$V_{\text{x,ATP}}(x) = \frac{K_{\text{PS}}}{2}(x - x_{\text{d}} - d_{\text{max}})^2 + F_{\text{ext}}x. \tag{4}$$

The minima of such a potential is located at x_{min}, where

$$x_{\text{min}} = d_{\text{max}} + x_{\text{d}} - \frac{F_{\text{ext}}}{K_{\text{PS}}}. \tag{5}$$

The average step size under this condition is then

$$x_{\text{min}} - x_{\text{d}} = d_{\text{max}} - \frac{F_{\text{ext}}}{K_{\text{PS}}}, \tag{6}$$

which decreases linearly with the applied force. Due to the periodicity of the dynein/microtubule interaction, the step size of dynein takes values of multiplicities of 8.1 nm. Using $d_{\text{max}} \approx 30$ nm and $K_{\text{PS}} \approx 0.04$ pN nm^{-1} and Eq. 6, the average step size can be calculated. For example, one can estimate from Fig. 8 *b* that the dominant step size is 32 nm when the external force is between 0 and 0.08 pN. It becomes 24 nm when F_{ext} is between 0.08 and 0.4 pN and further decreases to 16 nm when F_{ext} is between 0.4 and 0.72 pN. It finally reduces to 8 nm when F_{ext} is >0.72 pN. This estimation is in excellent agreement with experimental results, which showed that the averaged step size is ~25 nm for steps taken against external forces between 0 and 0.4 pN and is 16 nm for steps taken against external forces between 4 and 0.8 pN (21). The step size averaged over steps taken against a 0.8 pN or larger external force is 8 nm. The above can be explained in an approximate fashion through Scheme A1, where the free energy of binding of a poststroke dynein is represented by a saw-tooth-like potential (in the calculations a Morse type of

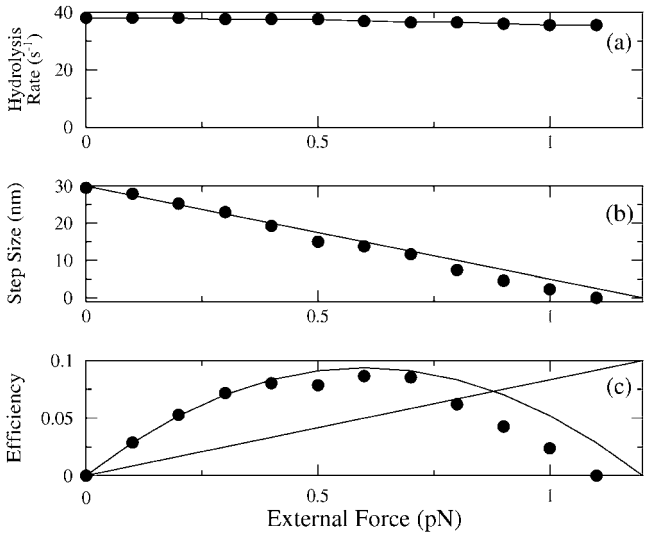

FIGURE 8 (*a*) Rate of ATP hydrolysis as a function of external load. (*b*, *solid circles*) Step sizes of dynein calculated as the ratio between the speed of dynein and the ATP hydrolysis rate; (*line*) average step size of dynein calculated using Eq. 6. (*c*, *solid circles*) Calculated thermodynamic efficiency using data points given in panel *b*; (*curved line*) calculated thermodynamic efficiency using Eq. 7; (*straight line*) thermodynamic efficiency of a tight coupling motor (such as kinesin) with a step size of 8.1 nm. The thermodynamic curve is only shown in the low external force for kinesin, because the chemomechanical coupling ratio is not determined at high forces, although the forward/backward ratios have been determined. The thermodynamic efficiency should also take a bell shape and will eventually vanish at its stall force (~8 pN).

potential with the same periodicity was used) and the prepowerstroke state potential is represented by the long-dashed curves. The conformational change in the α-coordinate is represented by the size of the shaded sphere and the translocation of dynein is along the *x*-direction. ATP binding (and/or ATP hydrolysis) removes dynein from the saw-tooth potential and generates the powerstroke for the translocation

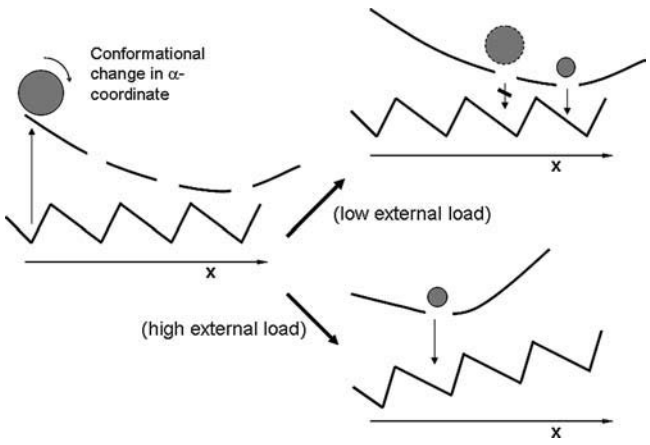

SCHEME A1 A schematic diagram illustrating the potential energy surfaces of dynein binding to microtubule as well as the motions along two reaction coordinates (see text for detailed discussion).

of dynein. The rebinding of dynein to the microtubule depends on the α-conformation of dynein (the size of the sphere in Scheme A1). When the external force is small, dynein translocates a long distance before it can rebind the microtubule, whereas when the external force is large, dynein rebinds microtubule after a short displacement (in Scheme A1, the size of the sphere is small enough for it to drop from the dashed curve to the solid saw-tooth-like line).

In principle, the decrease of the translocation speed with increasing external load (Fig. 5) can be either due to the slowed chemical transitions (e.g., through force-dependent ATP binding and/or ATP hydrolysis), or due to the slower walking speed of the motor, whichever is the rate-limiting step (34). Or, it can be resulted from a decreased step length with the turn over rate of ATP unchanged. To understand the origin of the linear dependence of the translocation speed on the external force, the rate of ATP hydrolysis is calculated as a function of the external forces. As seen from Fig. 8 *a*, the rate of ATP hydrolysis is largely constant in the external range of 0–1.1 pN. One can conclude from these observations that the decrease of the translocation speed of dynein in the presence of external forces is primarily due to the smaller step size under these conditions. This explanation of the force dependence of dynein motion is consistent with the experiments on the inner-arm axonemal dynein, which shows that even at very low concentrations of ATP (5 μM, so that ATP binding is rate limiting and the turnover rate of ATP is not influenced by the external force) the speed of motion decreases (as mentioned earlier, almost linearly) with increasing external force (33).

The average step size per ATP hydrolyzed can be calculated as the ratio between the velocity of translocation and the rate of ATP hydrolysis and is shown in Fig. 8 *b*, along with the result predicted by Eq. 6. The agreement between the step sizes calculated as the ratio between dynein speed and ATP hydrolysis rate and those predicted by Eq. 6 indicates that the hydrolysis of every ATP molecule leads to an attempt of forward motion, at least in the external force range of 0–1 pN. Moreover, under the assumption that the ATP turnover rate is insensitive to force, the experimental observation of a linear dependence of translocation speed on the external force for inner-arm axonemal dynein (33) would also indicate that the step size for a single step linearly depends on the external force, which is consistent with the results shown in Fig. 8 *b* and thus also with Eq. 6.

Although Eq. 6 predicts a step size larger than 32 nm when an external force is applied in the direction of dynein motion, one should be careful in drawing such a conclusion. At least when the assisting force is very large, there should be a structural limitation on how large a step the dynein can take, e.g., the interaction between the two heads of the dimeric dynein will certainly add constraints on how far they can be separated when one of the two is tightly bound to the microtubule. Nevertheless, it would be interesting to test this feature of this model by experiments.

A variable chemomechanical coupling ratio of dynein optimizes the thermodynamic efficiency in its cargo transportation in cells (21,22), which is analyzed in the following. Although the maximum thermodynamic efficiency that a dynein can achieve is much smaller than that by a kinesin, the larger steps that dynein takes in the presence of small external load makes dynein more efficient under these conditions. The thermodynamic efficiency of a dynein can be calculated as $\eta = F_{\text{ext}}x/n\Delta G$, where x is the step length of dynein, n is the average number of ATP molecules hydrolyzed per step taken, and ΔG is the chemical energy available from the hydrolysis of an ATP molecule. It has been shown earlier that the hydrolysis of every ATP leads to a single step, thus $n = 1$. Making use of Eq. 6, η can now be written as

$$\eta = \frac{1}{\Delta G}\left(F_{\text{ext}}d_{\max} - \frac{F_{\text{ext}}^2}{K_{\text{PS}}}\right). \quad (7)$$

In contrast, the thermodynamic efficiency of a tightly coupled motor such as kinesin is written simply as $\eta = F_{\text{ext}}d/\Delta G$ and $d = 8.1$ nm. Because $d_{\max} > d$, the thermodynamic efficiency is obviously larger for a dynein than for a kinesin when the external load F_{ext} is small. The thermodynamic efficiencies of dynein and kinesin are compared in Fig. 8 *c* for different values of external loads. The thermodynamic efficiency of dynein shown in Fig. 8 *c* was obtained using $\eta = F_{\text{ext}}d_{\text{ave}}/\Delta G$, where d_{ave} is average step length of dynein from Fig. 8 *b* as well as using Eq. 7. One noticeable feature of the dynein thermodynamic efficiency is that it is significantly larger than that of kinesin in the presence of smaller external load and is approximately constant when the external force is in the range of 0.2–0.8 pN.

In summary, this model predicts that dynein possesses a chemomechanical coupling mechanism that is both tight and loose. It is tight in the sense that the hydrolysis of every ATP molecule leads to a linear motion of the dynein so that higher ATP concentrations prevent dynein from sliding backward at small external forces (see Fig. 1 of Mallik et al. (21)), and is loose in that the length of step that dynein takes with every ATP hydrolyzed varies with external load. ATP hydrolysis without taking a step along microtubule is avoided by the ''tight'' coupling between the chemical reactions and the conformational change of dynein in α. On the other hand, the loose coupling between linear motion of dynein along the microtubule and the chemical reaction leads to a variable step length. The interplay of the tight and loose coupling discussed above makes dynein an efficient motor, in particular in the low external load regime. This unique chemomechanical coupling mechanism of dynein is likely to play important roles in living cells. The external force that a dynein has to work against in cells is more likely to be frictional than to be conservative unless the transportation is against a chemical potential gradient. When the force is purely frictional, the free-energy profile as a function of the x-coordinate is not altered by changes in friction. As a result the step size, dynein is capable of transporting cargoes of different frictions, thus of different sizes and/or shapes, with large steps and thus also a high efficiency. On the other hand, when the pathways of a dynein and a kinesin cross (they share the same track but move in opposite directions (1,3,23,35)) because kinesin can sustain a larger external force whereas dynein can take a longer step, dynein may be able to move to the side (bind to a different protofilament) and clear the road for kinesin. Therefore, a traffic jam can be avoided without losing the transportation of cargoes.

ATP concentration dependence of the stall force

As mentioned earlier, the stall force of dynein shows a strong dependence on the ATP concentration. The experimentally measured stall force at saturating concentrations of ATP is ~1.1 pN and decreases to ~25% of this value at low concentrations of ATP (~0.1 mM) (21). The experimental data (21) also show that when the external force approaches the stall force, the motor, instead of becoming immobile on the track, slips backward along the microtubule. The smaller force at which dynein starts to slip backward at lower ATP concentrations suggests that the overall binding of dynein to the microtubule is weaker at lower concentrations of ATP. It has been observed experimentally (29) that in the absence of nucleotide, there is very little diffusive motion of dynein on the microtubule track. With the presence of AMPPNP or ADP in solution, dynein also keeps strongly bound to the microtubule (29). However, when ATP is added to the system, besides directional translocation of dynein along the microtubule track, a significant portion of dynein molecules diffuse in both directions along microtubule. Because dynein with an ADP or an AMPPNP (an analog of ATP that does not hydrolyze) bound to the catalytic site has a high binding affinity to microtubule, the diffusive dynein species (dyneins that are weakly bound to microtubule) are likely generated after the hydrolysis of ATP and release of ADP. The conformation of the diffusive dyneins should also be different from those generated in the absence of nucleotide because the latter bind strongly to microtubule (29). A kinetic scheme that explains the observations mentioned above is given as follows:

$$\begin{aligned} &\text{D}(\text{D}^*) + \text{ATP} \leftrightarrow (\text{D.ATP}) \leftrightarrow (\text{D.ADP.Pi}) \\ &\quad \leftrightarrow (\text{D.ADP}) + \text{Pi} \leftrightarrow \text{D}^* + \text{ADP} + \text{Pi} \leftrightarrow \text{D} + \text{ADP} + \text{Pi} \end{aligned}$$

In the above kinetic scheme D* and D are both nucleotide-free dynein. D* is produced from the release of hydrolysis products and binds microtubule weakly. D binds microtubule strongly and has a conformation similar to that prepared in the absence of nucleotides in solution. Binding of ATP to both D and D*, although the rate constants might be different, generates a power stroke for the motion of dynein along the microtubule track.

The different species D* and D and their different binding affinities are represented in this model by different values of α. The binding between dynein and microtubule depends not only on the distance between dynein and its binding site on

microtubule but also on the conformation of dynein that is described by the reaction coordinate of conformational change, α. The α-values of the newly produced nucleotide-free dynein from the hydrolysis of ATP and the release of ADP-Pi are such that the dynein only binds microtubule weakly (see Eq. 14). The transition of D* to D is thus driven by the stronger binding of D to the microtubule.

When ATP concentration is high, the binding of ATP to dynein including D* is fast and the lifetime of the weak binding species D* is short. This shortening of the lifetime of the weak binding species reduces the probability for a dynein to take a backward motion under the influence of the external force. On the other hand, when ATP concentration decreases, the binding of ATP to D* is less frequent, and D* is subject to backward movements in the presence of small external loads. Therefore, the lower the ATP concentration, the more frequently does the backward motion occur and on average the smaller is the stall force.

APPENDIX

Potential energy functions

The expressions of potential energy functions $V(x,\alpha;i)$ for each of the chemical state i as well as other parameters used in the calculations are listed and discussed in this Appendix. For simplicity and to take into account the loose coupling between the motions along the two coordinates x and α, the potential energy of ATP and ADP states is assumed to take the form

$$V(x,\alpha;i) = V_x(x;i) + V_\alpha(\alpha;i), \tag{8}$$

where i represents either the ADP or the ATP state. To take into account the fact that a dynein at an ADP state binds strongly to the microtubule, and that the binding between dynein and microtubule has a periodicity of 8.1 nm, $V_x(x;ADP)$ is further assumed to be a Morse-type function and that the binding is the strongest at lattice sites k (of positions x_k), so that

$$V_x(x;ADP) = V_{ADP}\left(1 - \sum_k e^{-\left(\frac{x-x_k}{d}\right)^2}\right). \tag{9}$$

V_{ADP} in Eq. 9 is a constant describing the strength of binding and d is a constant that describes the decay length of the binding strength. Because it is known that dynein binds to the β-tubulin only (5,23), d is taken to be half of the length of a tubulin monomer, which is ~2 nm. A V_{ADP} of 5 kcal/mol is used in the calculations to be consistent with the tight binding between the ADP state of dynein and the microtubule. The exact value of V_{ADP} has little influence on the experimental results as long as it is 5 kcal/mol or larger.

When the system is at a prestroke state (in this scheme, the ATP state, although the assumption of any chemical state to be the prestroke state has no effect on the results of this article, except that the notation should be changed), a power-stroke term should be present in $V_x(x;ATP)$. In this study, a quadratic function is used to describe this prestroke free-energy term and for simplicity the binding at the microtubule lattice sites are neglected, because it is known that ATP binding releases dynein from microtubule (5). As a result,

$$V_x(x,ATP) = \frac{K_{ps}}{2}(x - x_d - d_{max})^2. \tag{10}$$

In Eq. 10, x_d is the position of dynein on the coordinate x where ATP binding occurs. The values of K_{PS} and d_{max} are given later.

We note that the quadratic function used here lacks the periodicity of the microtubule lattice, which would be required for a single particle diffusing on a track with a perfect translational symmetry. This symmetry can be broken either due to the structure of the microtubule, or it could be due to the interactions between the two monomers that are forming the dimeric motor protein. In the following, we illustrate how a potential of the form of Eq. 10 may arise due to the interactions between the two ''heads'' of a dimeric protein. We note that the exact nature of how the translational symmetry is broken has no influence on this model. It is well known that both myosin V and VI take steps that are multiple (but probably a constant number of) actin unit lengths. For a dimeric construction of dynein, the free energy of binding can be written as

$$V(x_1,x_2) = V_b(x_1) + V_b(x_2) + V_{int}(x_1,x_2). \tag{11}$$

In Eq. 11 $V(x_1,x_2)$ is the free energy of the dynein when it is bound with microtubule, $V_b(x_{1,2})$ is the binding energy between head one/two (at position $x_{1,2}$) and the microtubule and has a periodicity of 8.1 nm, and $V_{int}(x_1,x_2)$ is the energy that arises from the interaction between the two heads. When $V_{int}(x_1,x_2)$ is assumed to be a function of the distance between the two heads, it can be further written as $V_{int}(x_1-x_2)$. In the prestroke state of head one, it only binds the microtubule weakly (so that it can move along the microtubule). On the other hand, when head one detaches from microtubule the second head should bind the microtubule strongly so that the dynein molecule does not diffuse away from the track. As a result the term $V_b(x_1)$ can be neglected in comparison with $V_b(x_2)$ in Eq. 11. Further, because the very strong binding of the second head to the microtubule, $x_2$can be approximated as a constant. The interaction term $V_{int}(x_1-x_2)$ can be rearranged as $V_{int}(x_1+x_2-2x_2)$. Because $(x_1+x_2)=2x$, where $x$is the position of the center of mass of dynein on the microtubule, the free-energy function when one of two heads is at a prestroke state can be written as

$$V(x,x_2) = V_b(x_2) + V'_{int}(x - x_2). \tag{12}$$

Because one can use x_2 to define the initial position of dynein (pre-prestroke state or poststoke from the previous cycle) and x_2 is constant, one can further write Eq. 12 as $V(x) = V(x-x_2)$. When a quadratic function is assumed for $V(x)$, one has Eq. 10.

The free-energy term $V_\alpha(\alpha;i)$ is simply written as a quadratic function of α,

$$V_\alpha(\alpha;i) = \frac{K_{\alpha,i}}{2}(\alpha - \alpha_i)^2. \tag{13}$$

In Eq. 13 $K_{\alpha,i}$ is a constant and α_i denotes the location of the free-energy minimum of state i. Without any loss of generality, one can write the location of the free-energy minima for the ATP and empty states as $\alpha_{ATP} = 1$ and $\alpha_{emp} = 0$, respectively. The minimum free energy of the ADP state is assumed to occur at a value between 0 and 1, say $\alpha_{ADP} = 1/2$. Its exact position has very little influence on the calculated results. In this description, during every cycle of ATP hydrolysis reaction the minima of the potential of mean forces changes from 0 to 1 (binding of ATP) and then back to 0 again (release of products). Each of the chemical transitions is assumed to occur with a probability distribution peaked at the free-energy minima of its initial (reactant) state. A same value is used for the parameter $K_{\alpha,i}$ for all states. This value of $K_{\alpha,i}$ is chosen to be 15 kcal/mol/(unit length in α), so that the total free-energy change (the free-energy drop due to the power stoke plus the free-energy change along the α-coordinate) is close to the free energy available from the hydrolysis of one ATP molecule at cellular concentrations, which is ~11.6 kcal/mol. The exact value of $K_{\alpha,i}$ has very little influence on the calculated results.

As discussed in the main text, to account for the weak binding between dynein and microtubule in the poststroke state, the binding of an empty dynein and a microtubule is taken to be dependent on the dynein position along the x- as well as the α-coordinates. To take into account this property of dynein and for simplicity, the potential energy surface of an empty state is written as

$$V(x,\alpha;emp) = V_{emp}(x)V_{\alpha,emp}(\alpha). \tag{14}$$

The $V_{emp}(x)$ is taken to be the same as that given in Eq. 9 and $V_{\alpha,emp}(\alpha)$ is also taken to be a Morse-type potential with a minimum at $\alpha = 0$ and a decay length of 0.5, so that the binding of the empty dynein to microtubule is weak when α is removed from 0, the free-energy minimum of the empty state.

Maximum stall force and the power stroke generated by ATP binding

At vanishing external forces dynein takes steps of step lengths of a mixture of 16, 24, and 32 nm, with 32 nm being the largest step length observed in the experiments. A value of $d_{max} = 30$ nm was estimated based on these experimental results (21). This value of d_{max} is also consistent with other experimental observations (28). At high concentrations of ATP, the forward motion of dynein ceases when the applied force is large enough to cancel with the driving force produced by ATP binding. Therefore, when the externally load approaches the stall force, the step length of dynein approaches zero and the minima of the free energy of the ATP bound state moves toward x_d, namely $d(V_{x,ATP}(x)+F_{ext}x)/dx = 0$ at $x = x_d$. The maximum stall force $F_{s,max}$ at saturating concentrations of ATP was obtained from the experiments to be ~1.1 pN. When a potential in the form of Eq. 10 is used, K_{PS} is estimated to be ~0.02 pN nm^{-1} based on the values of d_{max} and $F_{s,max}$.

Rate parameters and diffusion constant

The binding rate constant of ATP to the dynein is taken to be $k_T = 7 \times 10^5$ M^{-1}s^{-1}, a value estimated from experiments (4) and is assumed to be the same for all values of α. When the experimentally measured K_d value of ~40 μM (35) was used, the ATP release rate is 30 s^{-1} at $\alpha = 0$ and $x = x_k$, where x_k is the position of the dynein binding site on the microtubule. The rate of ATP release at any other point (x, α) is calculated using $k_{-T}(\alpha, x) = k_{-T}\exp((\Delta V_{\alpha,x} - \Delta V_0)/k_BT)$, where $\Delta V_{\alpha,x}$ is the energy difference between the ATP bound state and the empty state at the given α and x, and ΔV_0 is its value at $\alpha = 0$ and $x = x_l$, x_l being the position of the dynein binding site on microtubule at which ATP binding occurs. The maximum rate of ADP release (at $\alpha = 1$) is assumed to be 50 s^{-1}. Because for most protein motors the Pi release rate tends to be large, it is assumed to be >100 s^{-1}. The rate constant k_{ij} for the chemical transition of $i \rightarrow j$ in the case of Pi and ADP releases are both assumed to follow $k_{ij} = k_{ij}^0\exp(-(\alpha-\alpha_i)^2)$, where k_{ij}^0 is the maximum rate constant at $\alpha = \alpha_i$. Both ADP and Pi binding was neglected in this study. The reason of assuming that the ADP and Pi release occurs with the highest rate only at certain values of α is to avoid chemical transitions to occur without taking physical steps.

The diffusion constant D_x was taken as the experimental value, which is ~2×10^4 nm^2 s^{-1}(29). The value of D_α is taken as 0.001 D_x, to make the time for a diffusion of 32 nm in the x-direction to be similar to the time it takes for the diffusion in the α-direction from 0 to 1. Although the exact value of $D_\alpha \sim 0.001\ D_x$ has only minor influence on the calculated results, a D_α much larger than the value used here reduces the step size of the dynein even at very small forces, resulted from a too-fast ATP hydrolysis compared to the physical translocation. A very small D_α (<0.0001 D_x), on the other hand, makes the overall reaction too slow and the speed of translocation is smaller than the experimental value. However, because the effect of choosing a larger D_α can be canceled by choosing a smaller chemical rate constant (in particular, the release rate of ADP), one should emphasize too much the exact values of these parameters.

Different behavior of different species of dynein

Experiments on dyneins of different origins revealed very different mechanical properties. For example, the inner-arm axonemal dynein (18) and the brain cytoplasm dynein 1 (28) considered in this study has a maximal stall force of 1–2 pN, whereas both the outer-arm dynein (19) and the yeast cytoplasm dynein have a stall force of 5–7 pN, very close to that of a kinesin. The inner-arm dynein but not the outer-arm dynein shows a linear dependence of microtubule gliding speed on the external force and the latter has a velocity-force curve that is downwardly convex (19). In a recent work on *Saccharomyces cerevisiae* cytoplasm dynein (36) it was found that MgADP is almost as efficient as MgATP in dissociating dynein from microtubule, which suggests that the dynein ADP state binds weakly to the microtubule. In that case, the backward motion of the ADP state should also be taken into account. At the zeros-order of approximation, it seems that the brain cytoplasm and the inner-arm dyneins are similar in their mechanical properties, although they have very different molecular construct. This model for the brain cytoplasm dynein 1 may also be applicable to an inner-arm dynein, but is less likely to be applicable to outer-arm or yeast cytoplasm dyneins.

Cooperativity between monomers

Due to the lack of structural information and experimental data on the interaction between the two heads of the dimeric cytoplasm dynein 1, instead of treating the movement of the two heads on the microtubule separately, the dynein is treated in this study as a single Brownian particle moving along the microtubule track. To understand more details of the motion of dynein, e.g., to distinguish a hand-over-hand mechanism from an inchworm one, a more detailed model with two interacting heads is in demand. Because the state of the binding of one head to the microtubule sets constraints on the motion (both along the track and off the track) of the second head, the inclusion of two heads explicitly in the model is also necessary for the understanding of processivity of this motor protein. It may also influence the fluctuation of position of the dynein and its motion on the track.

The author acknowledges a new faculty award from The Camille & Henry Dreyfus Foundation.

REFERENCES

1. Mallik, R., and S. P. Gross. 2004. Molecular motors: Strategies to get along. *Curr. Biol.* 14:R971–R982.
2. Burgess, S. A., and P. J. Knight. 2004. Is the dynein motor a winch? *Curr. Opin. Struct. Biol.* 14:138–146.
3. Welte, M. A. 2004. Bidirectional transport along microtubules. *Curr. Biol.* 14:R525–R537.
4. Samso, M., and M. P. Koonce. 2004. 25 angstrom resolution structure of a cytoplasmic dynein motor reveals a seven-member planar ring. *J. Mol. Biol.* 340:1059–1072.
5. Oiwa, K., and H. Sakakibara. 2005. Recent progress in dynein structure and mechanism. *Curr. Opin. Cell Biol.* 17:98–103.
6. Cross, R. A. 2004. Molecular motors: Dynein's gearbox. *Curr. Biol.* 14:R355–R356.
7. Koonce, M. P., and M. Samso. 2004. Of rings and levers: the dynein motor comes of age. *Trends Cell Biol.* 14:612–619.
8. Burgess, S. A., M. L. Walker, H. Sakakibara, K. Oiwa, and P. J. Knight. 2004. The structure of dynein-c by negative stain electron microscopy *J. Struct. Biol.* 146:205–216.
9. Burgess, S. A., M. L. Walker, H. Sakakibara, P. J. Knight, and O. Kazuhiro. 2003. Dynein structure and power stroke. *Nature.* 421:715–718.
10. Kon, T., M. Nishiura, R. Ohkura, R. Ohkura, Y. Y. Toyoshima, and K. Sutoh. 2004. Distinct functions of nucleotide-binding/hydrolysis sites in the four AAA modules of cytoplasmic dynein. *Biochemistry.* 43:11266–11274.
11. Takahashi, Y., M. Edamatsu, and Y. Y. Toyoshima. 2004. Multiple ATP-hydrolyzing sites that potentially function in cytoplasmic dynein. *Proc. Natl. Acad. Sci. USA.* 101:12865–12869.
12. Kikushima, K., T. Yagi, and R. Kamiya. 2004. Slow ADP-dependent acceleration of microtubule translocation produced by an axonemal dynein. *FEBS Lett.* 563:119–122.
13. Yildiz, A., M. Tomishige, R. D. Vale, and P. R. Selvin. 2004. Kinesin walks hand-over-hand. *Science.* 303:676–678.

14. Yildiz, A., J. N. Forkey, S. A. McKinney, T. Ha, Y. E. Goldman, and P. R. Selvin. 2003. Myosin V walks hand-over-hand: Single fluorophore imaging with 1.5-nm localization. *Science.* 300:2061–2065.

15. Schnitzer, M. J., K. Visscher, and S. M. Block. 2000. Force production by single kinesin motors. *Nat. Cell Biol.* 2:718–723.

16. Visscher, K., M. J. Schnitzer, and S. M. Block. 1999. Single kinesin molecules studied with a molecular force clamp. *Nature.* 400:184–189.

17. Nishiyama, M., H. Higuchi, and T. Yanagida. 2002. Chemomechanical coupling of the forward and backward steps of single kinesin molecules. *Nat. Cell Biol.* 4:790–797.

18. Sakakiara, H., H. Kojima, Y. Sakai, E. Katayama, and K. Oiwa. 1999. Inner-arm dynein c of Chlamydomonas flagella is a single-headed processive motor. *Nature.* 400:586–589.

19. Hirakawa, E., H. Higuchi, and Y. Y. Toyoshima. 2000. Processive movement of single 22S dynein molecules occurs only at low ATP concentrations. *Proc. Natl. Acad. Sci. USA.* 97:2533–2537.

20. Iyadurai, S. J., M. G. Li, S. P. Gilbert, and T. S. Hays. 1999. Evidence for cooperative interactions between the two motor domains of cytoplasmic dynein. *Curr. Biol.* 9:771–774.

21. Mallik, R., Carter, Lex, S. A., King, S., J. & Gross, S.P. 2004. Cytoplasmic dynein functions as a gear in response to load. Nature 427: 649–652.

22. Karplus, M., and Y. Q. Gao. 2004. Biomolecular motors: the F-1-ATPase paradigm. *Curr. Opin. Struct. Biol.* 14:250–259.

23. Mizuno, N., S. Toba, M. Edamatsu, J. Watai-Nishii, N. Hirokawa, Y. Y. Toyoshima, and M. Kikkawa. 2004. Dynein and kinesin share an overlapping microtubule-binding site. *EMBO J.* 23:2459–2467.

24. Wang, H. Y., and G. Oster. 1998. Energy transduction in the F_1 motor of ATP synthase. *Nature.* 396:279–282.

25. Xing, J. H., H. Y. Wang, C. von Ballmoos, P. Dimroth, and G. Oster. 2004. Torque generation by the Fo motor of the sodium ATPase. *Biophys. J.* 87:2148–2163.

26. Astumian, R. D., and I. Derenyi. 1999. A chemically reversible Brownian motor: application to kinesin and ncd. *Biophys. J.* 77:993–1002.

27. Inaba, K. 1995. ATP-dependent conformational-changes of dynein - evidence for changes in the interaction of dynein heavy-chain with the intermediate chain-1. *J. Biochem. (Tokyo).* 117: 903–907.

28. Shingyoji, C., H. Higuchi, M. Yoshimura, E. Katayama, and T. Yanagida. 1998. Dynein arms are oscillating force generators. *Nature.* 393:711–714.

29. Wang, Z. H., and M. P. Sheetz. 1999. One-dimensional diffusion on microtubules of particles coated with cytoplasmic dynein an immunoglobulins. *Cell Struct. Funct.* 24:373–383.

30. Levy, R. M., M. Karplus, and J. A. Mccammon. 1979. Diffusive Langevin dynamics of model alkanes. *Chem. Phys. Lett.* 65: 4–11.

31. Toba, S., and Y. Y. Toyoshima. 2004. Dissociation of double-headed cytoplasmic dynein into single-headed species and its motile properties. *Cell Motil. Cytoskeleton.* 58:281–289.

32. Shiroguchi, K., and Y. Y. Toyoshima. 2001. Regulation of monomeric dynein activity by ATP and ADP concentrations. *Cell Motil. Cytoskeleton.* 49:189–199.

33. Kojima, H., M. Kikumoto, H. Sakakibara, and K. Oiwa. 2002. Mechanical properties of a single-headed processive motor, inner-arm dynein subspecies-c of Chlamydomonas studied at the single molecule level. *J. Biol. Phys.* 28:335–345.

34. Tinoco, I., and C. Bustamante. 2002. The effect of force on thermodynamics and kinetics of single molecule reactions. *Biophys. Chem.* 101:513–533.

35. Ligon, L. A., M. Tokito, J. M. Finklestein, F. E. Grossman, and E. L. F. Holzbaur. 2004. A direct interaction between cytoplasmic dynein and kinesin I may coordinate motor activity. *J. Biol. Chem.* 279:19201–19208.

36. Mocz, G., M. K. Helms, D. M. Jameson, and I. R. Gibbons. 1998. Probing the nucleotide binding sites of axonemal dynein with the fluorescent nucleotide analogue 2 ′(3 ′)-O-(-N-methylanthraniloyl)-adenosine 5 ′-triphosphate. *Biochemistry.* 37:9862–9869.